Available online at www.sciencedirect.com

ScienceDirect

Energy Procedia 69 (2015) 523 – 531

Energy Procedia

International Conference on Concentrating Solar Power and Chemical Energy Systems, SolarPACES 2014

Experimental and numerical characterization of ceramic and metallic absorbers under lab-scale conditions

M.I. Roldán[a]*, A. Avila-Marin[b], M. Alvarez-Lara[b], J. Fernandez-Reche[a]

[a]*Plataforma Solar de Almería-CIEMAT, Ctra. de Senés, s/n, 04200 Tabernas, Almería, Spain*
[b]*Plataforma Solar de Almería-CIEMAT, Avda. Complutense 40, Madrid E-28040, Spain*

Abstract

Volumetric receiver technology has a huge potential for increase in the receiver and power block efficiencies by reducing the radiative thermal losses and increasing the temperature of the heat transfer fluid. With the aim of improving the thermal behavior of these types of receivers, CIEMAT-PSA is working at lab-scale on different configurations and geometries to optimize absorber behaviors. Furthermore, simplified Computational Fluid Dynamics (CFD) models have been developed to determine their feasibility for the prediction of the receiver experimental behavior and to analyze the heat transfer and thermal losses produced.

As part of this work, experimental results of both a SiC absorber and an alloy-601 one tested under lab-scale conditions, under similar outlet receiver temperatures, were assessed. Moreover, the numerical results obtained from a two dimensional (2D) CFD model, which considers thermal equilibrium between solid and fluid phases, have been presented for the selected experimental data. The deviation between the experimental thermal efficiency and the numerical one was lower than 10%, showing a good agreement for a first-approach CFD model. The average thermal efficiency reached under lab-scale conditions was around 90% in both cases.

Peer review by the scientific conference committee of SolarPACES 2014 under responsibility of PSE AG

Keywords: solar volumetric receiver; lab-scale tests; CFD modeling; thermal efficiency.

* Corresponding author. Tel.: +34- 950387800-839; fax: +34- 950365015.
E-mail address: mariaisabel.roldan@psa.es

Peer review by the scientific conference committee of SolarPACES 2014 under responsibility of PSE AG
doi:10.1016/j.egypro.2015.03.061

Nomenclature

c_p	specific heat capacity of the air	P_w	power removed by the cooling water
G_{peak}	irradiance peak of the Gaussian distribution	T_{in}	air temperature at the absorber inlet
m	mass air flow	T_{out}	air temperature at the absorber outlet
$P_{air\text{-}in\text{-}HE}$	air power at the heat-exchanger inlet	x	position in x-axis direction
P_{inc}	incident power on the absorber	y	position in y-axis direction (absorber depth)
$P_{loss\text{-}conduction\text{-}HE}$	conduction losses in the heat exchanger	α	absorptance
$P_{loss\text{-}conduction\text{-}REC}$	conduction losses in the receiver	ξ	optical extinction coefficient
$P_{loss\text{-}convection\text{-}HE}$	convection losses in the heat exchanger	σ_x	image descriptor to define the ellipticity
$P_{loss\text{-}convection\text{-}REC}$	convection losses in the receiver		
$P_{loss\text{-}radiation\text{-}HE}$	radiation losses in the heat exchanger		
$P_{loss\text{-}radiation\text{-}REC}$	radiation losses in the receiver		

1. Introduction

Central Receiver Systems (CRS) appear as an emerging option in the Solar Thermal Power Plants (STPP) market. The first generation of commercial STPP with CRS technology is based on technological developments matured after more than two decades of research, using cavity or external tube receivers with saturated steam and molten salts schemes, respectively. Newer developments are being implemented with superheated steam, Sierra Sun Tower in USA and Khi Solar One in South Africa, or larger plant sizes, Crescent Dunes (110MWe) and Ivanpah Solar Electric Generating Station (377MWe) in the USA.

CRS with volumetric-receiver technology using air as Heat Transfer Fluid (HTF), either atmospheric or pressurized, have not been marketed yet. However, it emerges as a promising scheme that could increase receiver and power block efficiencies, both reducing radiative thermal losses and raising the temperature of the HTF. There are two basic power plant schemes in volumetric receiver applications which can include the aforementioned benefits: open-loop receiver system with a Rankine cycle [1] or closed loop receiver system with Brayton cycle [2].

Among all HTFs, atmospheric air has advantages in terms of availability, cost and environmental impact. It can be heated up to temperatures around 700-to-800 ºC, generating steam at 480-540 ºC and 35-140 bar in a Heat Recovery Steam Generator (HRSG), which feeds a steam turbine paired with an electricity generator [3].

In the last decades, different designs and configurations of volumetric receivers have been tested [4] with the aim of proposing an alternative choice for more mature technologies (water/steam and molten nitrate salts). This type of receivers reached higher temperatures in the heat transfer fluid together with greater thermal efficiencies [5]. Nevertheless, there are still unresolved questions (i.e. materials durability, window design) that make CRS with volumetric receiver a non-attractive option to be implemented in the current STPP-market situation.

CIEMAT-PSA still considers that volumetric receivers will have the opportunity to be implemented in commercial power tower plants, but a step forward is required in this technology to compete with more advanced CRS technologies. In order to identify high-efficient configurations and geometries for absorbers used as volumetric receivers, CIEMAT-PSA is working at lab-scale on different configuration and geometries to optimize absorber behaviors. Moreover, CFD models are being performed on the basis of geometrical input and optical-thermal output parameters to predict the experimental behavior and to study the thermal distribution of each absorber configuration. Both theoretical analysis and experimental evaluation of the absorbers considered should match and represent a correct analysis that could be extrapolated to different working conditions. This paper describes both experimental and CFD works for re-SiC and alloy 601 absorbers under different operating conditions and similar outlet receiver temperatures.

2. Experimental

The main objective of this work is the lab-scale experimental evaluation of different volumetric-receiver configurations and the validation of the CFD model developed to predict their behavior. In order to obtain a first

comparison between a ceramic-volumetric-receiver sample and a metallic one, the configurations selected were those previously tested at larger-scale conditions [6-7].

2.1. Test facility

The facility is composed by four sub-systems designed for the lab-scale evaluation of different volumetric-receiver samples [8] (see Fig. 1):

- A 4-kW solar simulator made up of a xenon lamp and a parabolic concentrator. Further details about the xenon lamp have been described by [9-10].
- A receiver sub-system where the different volumetric absorbers are placed. The absorber temperature is monitored by 24 K-type thermocouples distributed in six sections (see Fig. 2), 1 S-type thermocouple, 1 T-type thermocouple, 2 PT100 surface sensors and an infrared camera.
- A helical air-water heat exchanger sub-system equipped with 4 PT100 sensors, 2 PT100 surface sensors, 1 T-type thermocouple, a water mass flow-rate measurement, and a pump.
- An extraction sub-system with 2 PT100 sensors, an air mass flow-rate measurement, and a blower.

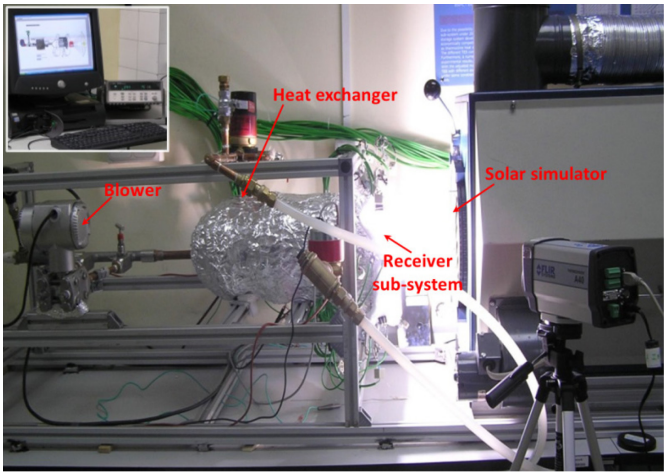

Fig. 1. Test facility for the thermal evaluation of open volumetric receivers with a 4-kW xenon arc lamp

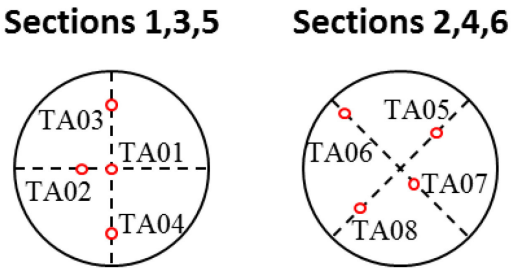

Fig. 2. Thermocouple location in each section.

2.2. Materials, samples and tests conditions

The materials selected as baseline were those used in HiTRec [6] and TSA receivers [7], recrystallized SiC and alloy 601, due to its appropriate performance for ceramic and metallic receivers, respectively.

The ceramic material consisted of a honey-comb recrystallized-SiC module with squared channels of 2 mm on each side distributed throughout the material and a porosity of 0.495. In order to study the SiC receiver, a sample of 60 mm in diameter and 44 mm thick was tested at the focal plane of the solar simulator, with a heat-flux peak of nearly 2000 kW/m^2, which corresponds to stagnation temperatures above 2400 K. In contrast, the metallic material was composed of a coiled knit-wire mesh of alloy 601, with a porosity of 0.974. This metallic sample had the same dimensions than the ceramic one and was tested at lower peaks, between 800 and 1300 kW/m^2, which correspond to stagnation temperatures in between 1900-2200 K.

For each absorber, three tests with the same air flow were performed to ensure that the absorber behavior is consistent with this parameter. The air-velocity range considered for the SiC absorber was between 1.1 m/s and 0.5 m/s, and the range of around 0.9-0.4 m/s for the alloy-601 material. These velocities were chosen to assure similar outlet receiver temperatures for both absorbers. The experimental evaluation was developed using one of the three tests carried out at the same conditions.

2.3. Experimental data evaluation

For the thermal evaluation of each absorber tested, conduction losses through the metallic tube and the ceramic blanket, together with convection and radiation losses through the aluminum foil, were considered both for the heat exchanger (HE) and for the volumetric receiver (REC) by the location of several PT100 sensors along the outer wall. The evaluation of the power gained by the air at the absorber outlet ($P_{air\text{-}out\text{-}ABS}$) is defined by the following expression:

$$P_{air-out-ABS} = P_{air-in-HE} + P_{loss-conduction-REC} + P_{loss-convection-REC} + P_{loss-radiation-REC} \quad (1)$$

The air power at the heat-exchanger inlet has been evaluated by:

$$P_{air-in-HE} = P_w + P_{loss-conduction-HE} + P_{loss-convection-HE} + P_{loss-radiation-HE} \quad (2)$$

The thermal efficiency (η) of the absorber was used to validate the CFD model for each case and was calculated using the following equation [11]:

$$\eta = \frac{m \cdot \int_{T_{in}}^{T_{out}} c_p dT}{P_{inc}} \cdot 100 = \frac{P_{air-out-ABS}}{P_{inc}} \cdot 100 \quad (3)$$

3. CFD simulations

A two-dimensional CFD model has been developed for each absorber in order to obtain a first approach of the receiver behavior, minimizing the computational cost. The receiver longitudinal profile has been defined as the solution domain, which consists of the absorber material, the receiver frame where the absorber is placed, the ambient-air area, and the heated-air zone (Fig. 3). The frame is covered by an insulating material, which is not included in the domain to avoid the increase of the computational cost. Thus, thermal losses have been considered as a boundary condition of the frame outer wall defined as the lost heat flux.

The selected mesh is built of quadrilateral cells, whose equiangle-skew value is included in the range of 0-0.25. It means that the mesh quality is excellent, according to [12].

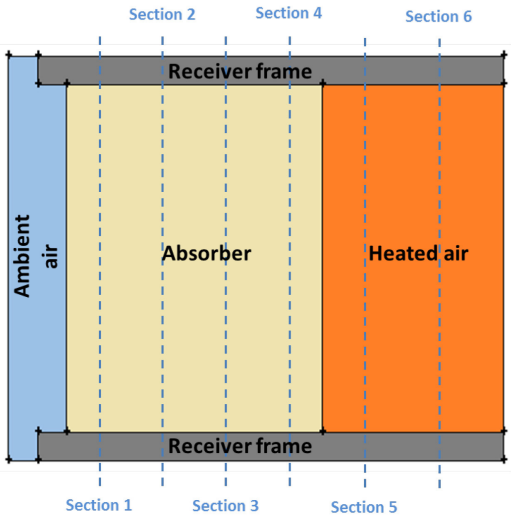

Fig. 3. Solution domain and measurement sections.

Conservation laws determine the fluid dynamics behavior [13]; therefore, the proposed CFD model has required solving the continuity, momentum [14] and energy [15] equations adapted to the assumptions considered in this study: steady-state flow condition and negligible gravitational force due to the air flow forced by the extraction unit.

The boundary conditions have been determined according to the steady state selected from the experimental data registered during each test. The mass flow and temperature of the fluid have been fixed as the air inlet conditions. CFD simulations have considered the heat-flux distribution for each case by the analysis of CCD-camera images [16] and each simulation has included the thermal losses produced in the absorption of the incoming radiation by the user defined function (UDF) described for the volumetric heat source, which has been defined in the absorber sub-domain. The UDF has been described by [5]:

$$Q(x,y)=\left(G_{peak}\cdot\exp\left(-\frac{1}{2}\cdot\left(\frac{x^2}{\sigma_x^2}\right)\right)\right)\cdot\alpha\cdot\xi\cdot\exp(-\xi\cdot y) \tag{4}$$

The first term of Equation (4) defines the irradiance distribution offered by the solar simulator obtained from the analysis of the recorded images. The absorber retains a part of this heat flux depending on its absorptance, and the degradation of the heat-flux along the receiver depth is determined by the extinction coefficient following an exponential pattern.

4. Evaluation procedure

The measurements of different thermocouples located in six sections along the sample were compared with the numerical results obtained from each 2D model (Fig. 2, Fig. 3). These data correspond to a quasi-steady state selected from each test. In the comparison, the measurement uncertainty and the one obtained for the numerical data were considered. The uncertainty of the numerical data was evaluated considering a deviation of 5% in the heat-flux peak measured. The limit values of the flux-peak range have been implemented in the Gaussian distribution of the irradiance, which was used as the volumetric heat source. Additionally, the thermal efficiency was evaluated for both experimental data and numerical result in order to define the absorber behavior taking into account that both absorbers have been tested under similar outlet receiver temperatures.

5. Results and discussion

Fig. 4 and Fig. 5 depict experimental data and numerical results for the SiC absorber and the alloy-601 one, respectively. Both figures show a high deviation between experimental and numerical data at the first transversal section, which is enhanced with the increase of the heat-flux peak of the irradiance distribution. Therefore, it can be concluded that thermocouples TA01 and TA02, located in this transversal section, are directly irradiated and their measurements are overestimated. Consequently, the results obtained for the first section have not been considered in the comparison between experimental and numerical data of each absorber.

It has also been observed that the higher absorber porosity, the more homogeneous longitudinal thermal profile is obtained. Thus, the SiC-absorber longitudinal thermal distribution is less homogeneous than the metallic-absorber one because the lower porosity reduces the radiation penetration along the absorber depth (see Fig.4 and Fig. 5).

Furthermore, some experimental measurements have been influenced by the solid temperature because, in some cases, the thermocouple can be located near the solid-wall area. This effect can be found in both absorbers (Fig. 4 and Fig. 5). However, numerical results are in good agreement with the experimental data at the absorber outlet, when solid and fluid tend to reach the thermal equilibrium. In this sense, the approach of the local thermal non-equilibrium model is proposed for more detailed porous-material analyses.

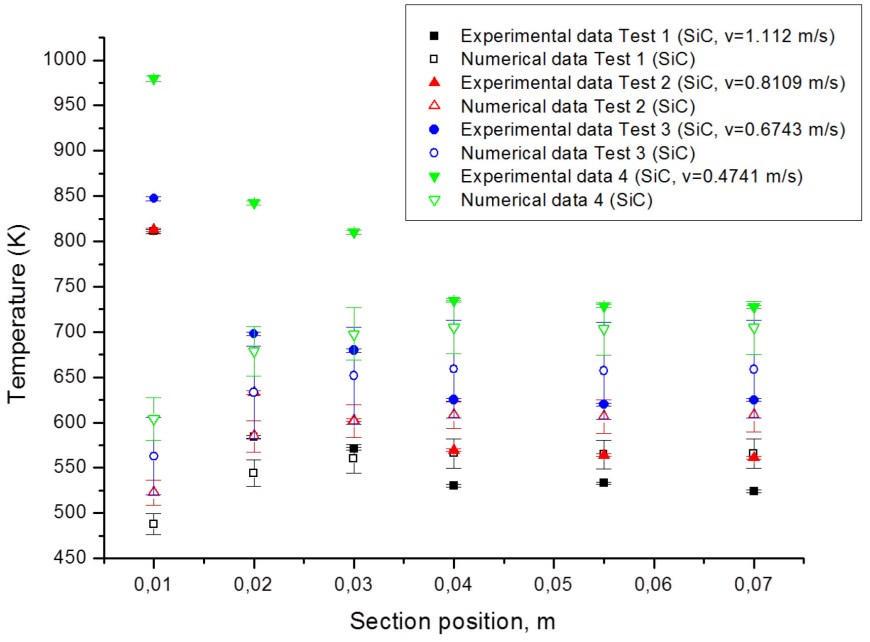

Fig. 4. Comparison between experimental and numerical data for the SiC absorber.

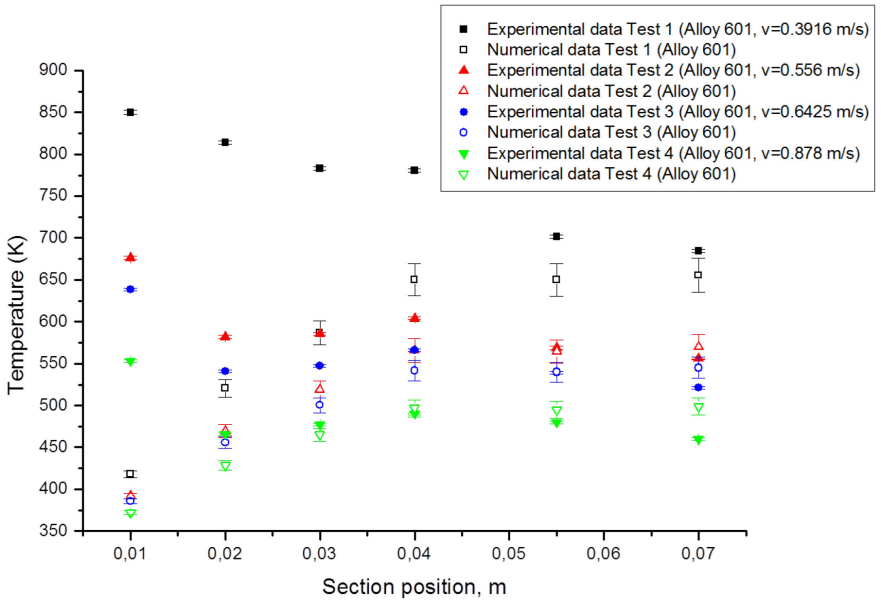

Fig. 5. Comparison between experimental and numerical data for the alloy-601 absorber.

Moreover, the thermal distribution obtained from the simulations shows a maximum-temperature area located at the center of the ceramic absorber. This is because the heat flux is mainly transferred along the ceramic-absorber depth, whereas the metallic material presents a more homogeneous transversal profile. The porosity, the heat exchange surface and the characteristic properties of each material influence the absorber thermal behavior. Nevertheless, both absorbers reach higher temperatures at lower fluid velocities.

In both cases, numerical and experimental results have determined average deviations lower than 10%, which means a good first approach of the CFD model simplified by the two-dimensional geometry and the local thermal equilibrium assumption. Higher deviations were caused by experimental thermal losses throughout the receiver tube and misalignment of the thermocouples located in the receiver sub-system. Figure 6 shows the position of the thermocouples after the tests compared to the initial position (red dashed lines).

The 0.5-mm diameter K-thermocouples are located inside a stainless steel tube to position them in the correct place. Due to the reduced diameter of the thermocouples, they can be placed easily within the absorbers. Furthermore, their location in the heated area (Fig. 3) could not be so precise because each position could change when the air was flowing through the receiver, as can be checked in Figure 6.

Table 1 includes the velocities used as boundary condition, the air temperatures at the receiver outlet, and the thermal efficiencies evaluated for each test at steady state, both experimental and numerical. It has been observed that the maximum deviation of the efficiency was around 10%. In both cases, the deviation between numerical and experimental values increases with the decreasing air velocity. Thus, the thermal profile is more homogeneous at higher air velocities, obtaining a lower difference between experimental and numerical data. Therefore, the inlet temperature considered for the evaluation of the numerical efficiency presents a greater deviation respect to the experimental one at lower velocities, which influences the efficiency value obtained.

Furthermore, the incident heat flux, which was impinging on the sample surface, caused the higher differences for the alloy-601 absorber. When the SiC absorber is tested in the focal plane of the solar simulator, the real heat-flux distribution presents almost a perfect Gaussian shape (Fig. 7a). Therefore, it can be transformed into a 2D Gaussian distribution without any uncertainty. Nevertheless, the alloy-601 absorber is tested far from the focal plane of the solar simulator and its heat-flux distribution is not as symmetric as the one obtained at the focal plane (Fig. 7b). This fact introduces some uncertainties into the 2D Gaussian distribution used for this absorber sample.

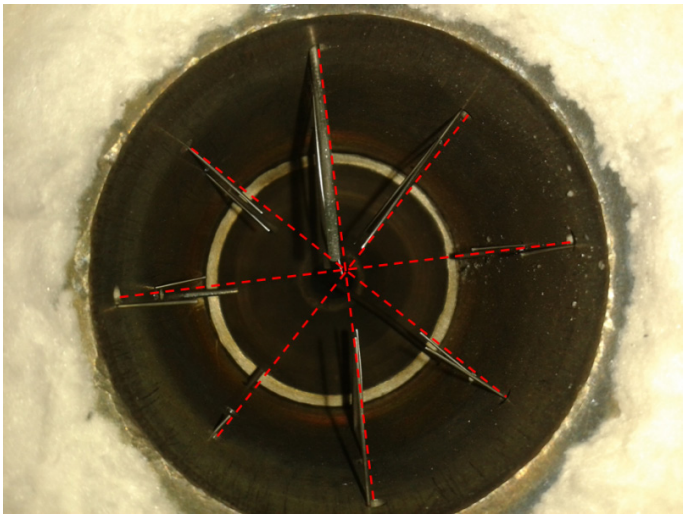

Fig. 6. Thermocouples position after the tests compared to the initial position (red dashed lines).

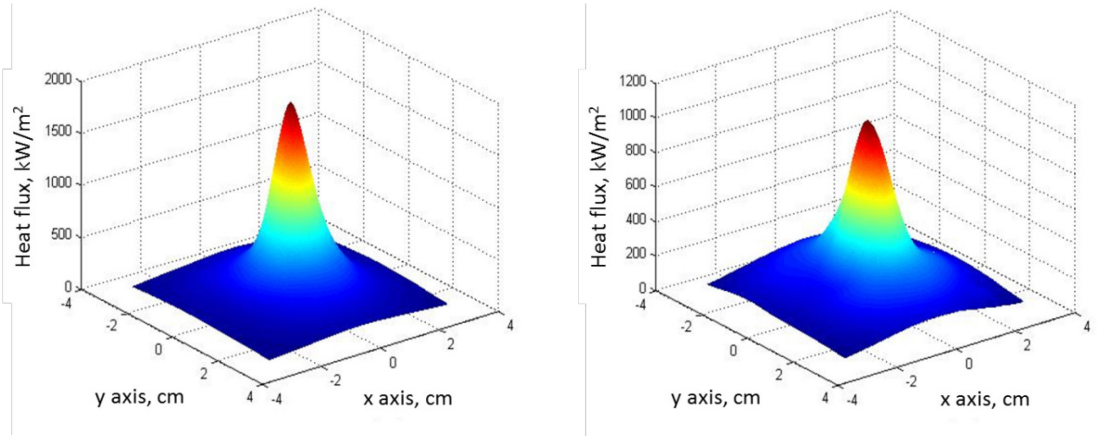

a) b)

Fig. 7. Irradiance distribution for the ceramic (a) and metallic (b) absorbers.

Table 1. Main experimental and numerical results.

Test	Velocity (m/s)	Temperature measured at the receiver outlet, K	Numerical temperature at the receiver outlet, K	Experimental efficiency (%)	Numerical efficiency (%)	Deviation (%)
1 (SiC)	1.1120	556	557	97.77	98.35	0.59
2 (SiC)	0.8109	613	612	89.35	88.92	0.48
3 (SiC)	0.6743	668	661	94.43	92.60	1.93
4 (SiC)	0.4741	777	730	89.88	80.64	10.27
1 (Alloy 601)	0.3916	761	719	84.57	76.15	9.95
2 (Alloy 601)	0.5560	647	622	89.62	82.55	7.89
3 (Alloy 601)	0.6425	605	593	89.03	85.16	4.34
4 (Alloy 601)	0.8780	532	536	88.97	90.64	1.88

6. Conclusions

Two samples of different absorber materials have been tested under several lab-scale conditions for similar outlet receiver temperatures. These results have been well reproduced by a first-approach 2D-CFD model at steady state, taking into account the fluid temperature at the absorber outlet. In order to develop a more detailed porous-material study in the future, a local thermal non-equilibrium model is proposed.

The thermal profiles obtained were more homogeneous in the metallic absorber than the ones showed by the ceramic material due to the higher porosity, the greater heat exchange surface, the deeper penetration of the radiation of the metallic configuration and the physical properties of each material. Therefore, the volumetric effect is enhanced by the alloy-601 absorber instead of the greater influence of the air flow through the sample.

The average thermal efficiency reached under lab-scale conditions was around 90% in both cases, with average deviations lower than 10%.

7. Future work

The analysis of other absorber configurations which combine gradual porosities and different materials was proposed in order to determine the optimum volumetric receiver, whose behavior is more accurately predicted by a local thermal non-equilibrium model.

Acknowledgements

The authors wish to thank “Comunidad de Madrid” and “European Social Fund” for its financial support to the SOLGEMAC Project through the Programme of Activities between Research Groups (S2009/ENE-1617). The authors also want to thank Mr. F. Sanchez for its work in the installation.

References

[1] Romero M, Buck R, Pacheco JE. An update on solar central receiver systems, projects, and technologies. J Sol Energ-T ASME 2002; 124: 98 – 108.
[2] Kribus A, Zaibel R, Carey D, Segal A, Karni J. A solar driven combined cycle power plant. Sol Energy 1998; 62: 121 – 129.
[3] Romero M, Zarza E. Handbook of energy efficiency and renewal energy, chapter 21: concentrating solar thermal power. CRC Press; 2007.
[4] Avila-Marin A. Volumetric receivers in solar thermal power plants with central receiver system technology: a review. Sol Energy 2011;85:891–910.
[5] Roldán MI, Smirnova O, Fend T, Casas JL, Zarza E. Thermal analysis and design of a volumetric solar absorber depending on the porosity. Renew Energ 2014;62:116-128.
[6] Hoffschmidt B, Téllez F, Valverde A, Fernández J, Fernández V. Performance evaluation of the 200-kWth HiTRec-II open volumetric air receiver. J Sol Energ-T ASME 2003;125:87-94.
[7] Meinecke W, Cordes S. Phoebus technology program solar air receiver (TSA) – operational experience and test evaluation of the 2.5 MWth volumetric air receiver test facility at the Plataforma Solar de Almeria. In: Proceeding of the 7th International Symposium on Solar Thermal Concentrating Technologies; 1994. p. 943–957.
[8] Avila-Marin A. et al. Experimental results of gradual porosity wire mesh absorber for volumetric receivers. Energy Procedia, Volume 49, 2014, Pages 275-283
[9] Petrasch J, Coray P, Meier A, Brack M, Häberling P, Wuillemin D, Steinfeld A. A Novel 50 kW 11000 suns High-Flux Solar Simulator Based on an Array of Xenon Arc Lamps. J Sol Energ-T ASME 2007; 129: 405 – 411.
[10] Gomez F, Gonzalez-Aguilar J, Romero M. Experimental 3D flux distribution of a 7 kWe solar simulator. 17th SolarPACES Conference Proceedings, Granada, Spain, 2011.
[11] Haeger M, Keller L, Monterreal R, Valverde A. Phoebus Technology Program Solar Air Receiver (TSA): Operational experiences with the experimental set-up of a 2.5 MW_{th} volumetric air receiver (TSA) at the Plataforma Solar de Almería. Report: PSA-TR02/94; 1994.
[12] Fluent-Inc. The Gambit graphical user interface (Chapter 3). In: Gambit 2.2 user’s guide. Lebanon, NH: Fluent-Inc; 2004.
[13] Blazek J. Computational fluid dynamics: principles and applications. 2nd ed. Elsevier; 2005.
[14] Batchelor GK. An introduction to fluid dynamics. Cambridge: University Press; 1967.
[15] Fluent-Inc. Modeling heat transfer (Chapter 12). In: Fluent 6.2 user’s guide. Lebanon, NH: Fluent-Inc; 2005.
[16] Roldán MI, Monterreal R. Heat flux and temperature prediction on a volumetric receiver installed in a solar furnace. Appl Energ 2014; 120: 65-74.